

3D semiconducting nanostructures via inverse lipid cubic phases.

Article

Published Version

Creative Commons: Attribution 4.0 (CC-BY)

Open Access

Burton, M. R., Lei, C., Staniec, P. A., Terrill, N. J., Squires, A. M., White, N. M. and Nandhakumar, I. S. (2017) 3D semiconducting nanostructures via inverse lipid cubic phases. *Scientific Reports*, 7 (1). 6405. ISSN 2045-2322 doi: <https://doi.org/10.1038/s41598-017-06895-5> Available at <https://centaur.reading.ac.uk/71878/>

It is advisable to refer to the publisher's version if you intend to cite from the work. See [Guidance on citing](#).

To link to this article DOI: <http://dx.doi.org/10.1038/s41598-017-06895-5>

Publisher: Nature Publishing Group

All outputs in CentAUR are protected by Intellectual Property Rights law, including copyright law. Copyright and IPR is retained by the creators or other copyright holders. Terms and conditions for use of this material are defined in the [End User Agreement](#).

www.reading.ac.uk/centaur

CentAUR

Central Archive at the University of Reading

SCIENTIFIC REPORTS



OPEN

3D semiconducting nanostructures via inverse lipid cubic phases

M. R. Burton¹, C. Lei¹, P. A. Staniec⁴, N. J. Terrill¹, A. M. Squires³, N. M. White² & Iris S. Nandhakumar¹

Received: 5 April 2017

Accepted: 19 June 2017

Published online: 25 July 2017

Well-ordered and highly interconnected 3D semiconducting nanostructures of bismuth sulphide were prepared from inverse cubic lipid mesophases. This route offers significant advantages in terms of mild conditions, ease of use and electrode architecture over other routes to nanomaterials synthesis for device applications. The resulting 3D bicontinuous nanowire network films exhibited a single diamond topology of symmetry $Fd\bar{3}m$ (Q_{227}) which was verified by Small angle X-ray scattering (SAXS) and Transmission electron microscopy (TEM) and holds great promise for potential applications in optoelectronics, photovoltaics and thermoelectrics.

Over the past few years the emergence of synthetic strategies and fabrication technologies that afford control over the architecture of matter at nanometer length scales has provided a new tool kit for engineering functionality in materials. In particular the three-dimensional (3D) nanostructuring of metals and semiconductors has resulted in enhanced optical, magnetic and electronic properties yielding new devices and device concepts. 3D nanowire networks represent a good example and are of great technological importance for many applications including energy harvesting¹, sensors², energy storage^{3,4}, solar cells⁵, optoelectronics⁶ and electrocatalysis⁷. Hence there is an urgent need for developing approaches to their fabrication. Most of the methods reported to-date involve the use of hard templates such as porous alumina membranes (AAO)⁸ or polymeric substrates such as e.g. polycarbonate⁹ that act as templates for (either chemical or electrochemical) deposition of the respective material. The main limitations associated with these approaches is that these templates require multiple and often complex fabrication steps and can only be removed in either acids, sodium hydroxide (NaOH) or organic solvents such as dichloromethane or dimethylformamide^{7,10} which raises safety and environmental concerns. These limitations can be overcome by using soft-templating approaches such as diblock copolymers¹¹ or amphiphilic surfactants¹². Diblock co-polymers for example have been used to produce gyroid networks of titania for applications in hybrid heterojunction solar cells¹³ and dye-sensitised solar cells⁵. The fabrication of diblock co-polymer templates however also involves synthetically complex steps and above all is very time-consuming, often taking several days^{5,13}. This has prompted us to explore whether inverse cubic lipid mesophases could provide an alternative fabrication method for 3D semiconductor nanostructures.

In the present study highly ordered 3D bicontinuous nanowire network films of the semiconductor compound bismuth sulphide (Bi_2S_3) were prepared by electrodeposition through inverse lipid cubic phases of phytantriol at room temperature under mild aqueous conditions. A combination of SAXS and TEM in conjunction with Matlab simulations and Fast Fourier Transforms (FFTs) has been utilised to verify the formation of a single diamond topology bismuth sulphide films with symmetry $Fd\bar{3}m$ (Q_{227}) from a double diamond phytantriol template of symmetry Q_{224} .

Bi_2S_3 has attracted considerable attention due to its potential for applications within photovoltaics^{14,15} and thermoelectric coolers¹⁶ given its direct band gap of 1.3 eV and positive photoconductivity. Thin films of Bi_2S_3 have been prepared by either chemical bath deposition¹⁶ or spray pyrolysis¹⁷, whilst nanowires as well as nanorod films were grown by hydrothermal synthesis¹⁸ or solventless thermolysis¹⁹. These methods necessitate elevated temperatures for successful synthesis and do not produce ordered and highly interconnected 3D nanostructures that are suitable for incorporation into devices. Whilst the electrochemical fabrication of Bi_2S_3 has been reported, literature coverage is extremely limited^{20–23} and to the best of our knowledge there are currently no studies on the formation of ordered nanowire networks of Bi_2S_3 films from bicontinuous cubic lipid phases. The use of inverse cubic lipid mesophases for the preparation of nanostructured semiconductors such as Bi_2S_3 has a number of distinct advantages over other routes to nanomaterial synthesis as illustrated in this study: Semiconductor

¹School of Chemistry, University of Southampton, Southampton, SO17 1BJ, UK. ²Electronics and Computer Science, University of Southampton, SO17 1BJ, Southampton, UK. ³Department of Chemistry, University of Reading, Reading, RG6 6AD, UK. ⁴Diamond Light Source, Diamond House, Harwell Science and Innovation Campus, Didcot, Oxon, OX11 0DE, UK. Correspondence and requests for materials should be addressed to I.S.N. (email: iris@soton.ac.uk)

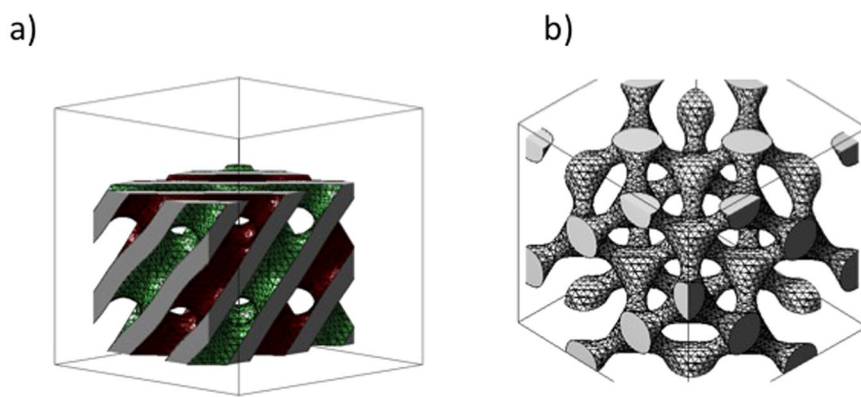


Figure 1. Schematic representation of (a) bicontinuous double diamond Q_{II} cubic phase of phytantriol displaying the two water channels in green and red and (b) single diamond bismuth sulphide nanostructure generated by MATLAB.

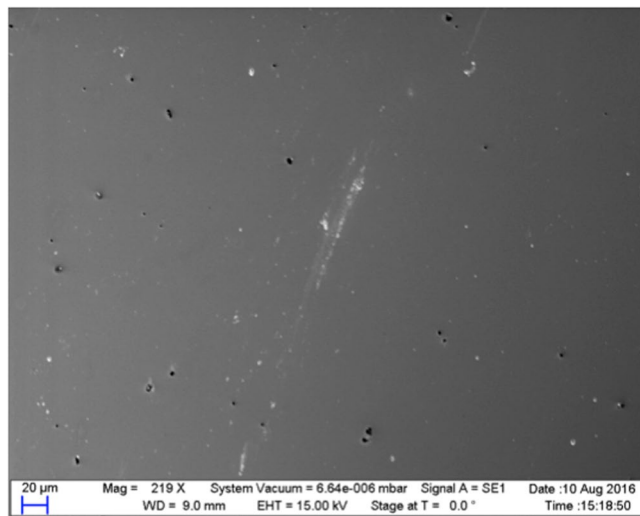


Figure 2. Scanning electron microscopy images of a bismuth sulphide film electrodeposited through a phytantriol template from an electrolyte solution containing 100 mM $Bi(NO_3)_3$, 100 mM $Na_2S_2O_3$ and 200 mM EDTA in deionised water. The film was deposited potentiostatically at a potential of -0.4 V vs. SCE for 4 hours.

compounds as can be deposited at room temperature, under chemically mild aqueous conditions. The templating process faithfully replicates the size and geometry of the template whilst the templates themselves can be prepared, and removed post-templating, by simple one-step processes using water or ethanol, making the entire process green, cost-effective and compatible with a range of substrate materials for device fabrication. The ability to fabricate 3D semiconductor nanostructures such as Bi_2S_3 with a bicontinuous cubic morphology will be highly attractive for many applications such as photovoltaics, thermoelectrics and optoelectronic as these materials have displayed enhanced charge transfer²⁴ and tunable phononic²⁵ and photonic bandgaps²⁶.

The phase diagram of phytantriol has previously been studied in detail by Baraukas *et al.*²⁷ and there are three symmetries of bicontinuous cubic structures that could be identified: the gyroid (G), double diamond (D), and primitive (P) surfaces corresponding to the space groups Ia3d (Q_{230}), Pn3m (Q_{224}), and Im3m (Q_{229}), respectively. For illustration, the bicontinuous double diamond phase is depicted in Fig. 1: This contains a single lipid bilayer on either side of which lie branching networks of nanometre-sized water channels.

Methods

Nanowire network films of bismuth sulphide were prepared by potentiostatic electrodeposition at a potential of -0.4 V vs SCE from an electrolyte containing 100 mM $Bi(NO_3)_3$, 100 mM $Na_2S_2O_3$ and 200 mM EDTA through phytantriol modified gold (Au) DVDs (Delkin Devices). Bismuth sulphide electrolytes were prepared by mixing the bismuth and sulphide precursors along with EDTA in dissolved water (Merck Millipore Milli-Q Gradient A10 Ultrapure water purification system, $18.2\text{ M}\Omega\text{ cm}$) over night. The solution was then left to settle for 2 days to allow a formed black precipitate to settle. A clear electrolyte solution was then separated and bubbled through with Argon for a minimum of 20 minutes, to remove dissolved oxygen. The two plastic layers of the DVD were

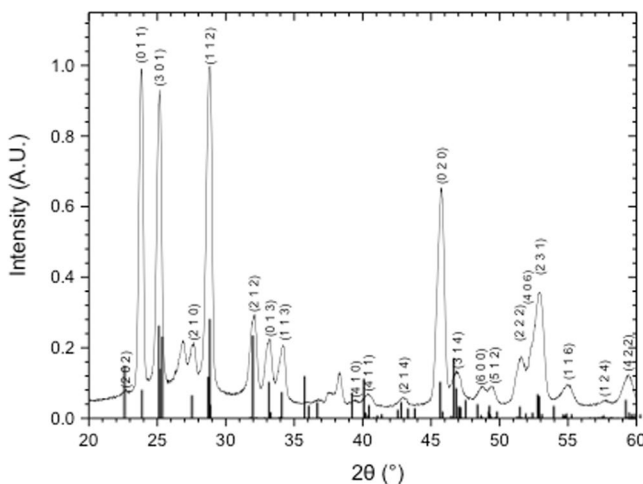


Figure 3. Grazing incidence x-ray diffraction scan of a bismuth sulphide film electrodeposited through a phytantriol template with superimposed pdf card 9007375 for Bismuthinite from the crystallographic open database.

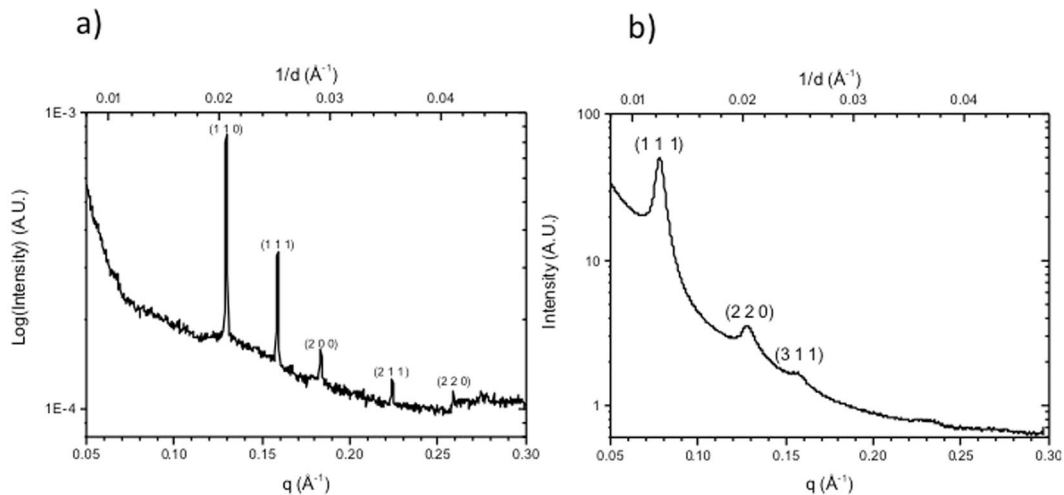


Figure 4. (a) 1D integrated SAXS patterns of a phytantriol coated gold foil immersed in 100 mM $\text{Bi}(\text{NO}_3)_3$, 100 mM $\text{Na}_2\text{S}_2\text{O}_3$ and 200 mM EDTA in deionised water and (b) of a bismuth sulphide film electrodeposited through a phytantriol template. The film was deposited potentiostatically at a potential of -0.4 V vs. SCE for 4 hours.

separated using mechanical force. The exposed gold layer disc was cut into $1.5\text{ cm} \times 1.5\text{ cm}$ using scissors. Cu tape was used to make an electrical contact and polyimide tape was used to isolate a $10\text{ mm} \times 10\text{ mm}$ working electrode area. The working electrode was dip coated in a solution of phytantriol and ethanol 1:2 by weight, allowed to dry for 30 minutes prior to being immersed in the electrolyte and was allowed to hydrate for 30 minutes in the electrolyte prior to electrodeposition. Films were deposited potentiostatically at a potential of -0.4 V vs. SCE for 4 h. A saturated calomel reference electrode and a Pt gauze counter electrode were used. Post deposition films were washed for a minimum of 30 minutes in ethanol.

A Zeiss EVO LS25 ESEM scanning electron microscope (SEM) with an Oxford Instruments energy dispersive x-ray spectrometer attachment was used to determine surface topography and composition of the Bi_2S_3 deposits. Accelerating voltages up to 15 KV were applied and images recorded with a secondary electron detector. Samples were mounted as deposited (on Au DVDs) on an 18 mm SEM clip specimen mount (agar scientific). XRD Grazing incidence scans, where the source is held at a constant shallow angle to the sample and the detector is scanned through theta values, were conducted on the nanotemplated films. A Rigaku SmartLab X-Ray diffractometer was used to obtain diffraction patterns. The Rigaku Smartlab uses $\text{Cu K}\alpha$ radiation with a wavelength of 1.5406 \AA . Small angle x-ray scattering measurements were carried out at Diamond light source on beamline I22 with beam energy and size of 12.4 KeV and $320\text{ }\mu\text{m} \times 80\text{ }\mu\text{m}$ respectively. A Pilatus 2 M detector²⁸ was used to collect data over the q range of 0.05 \AA^{-1} – 0.30 \AA^{-1} . Calibration was achieved by using a silver behenate²⁹ sample.

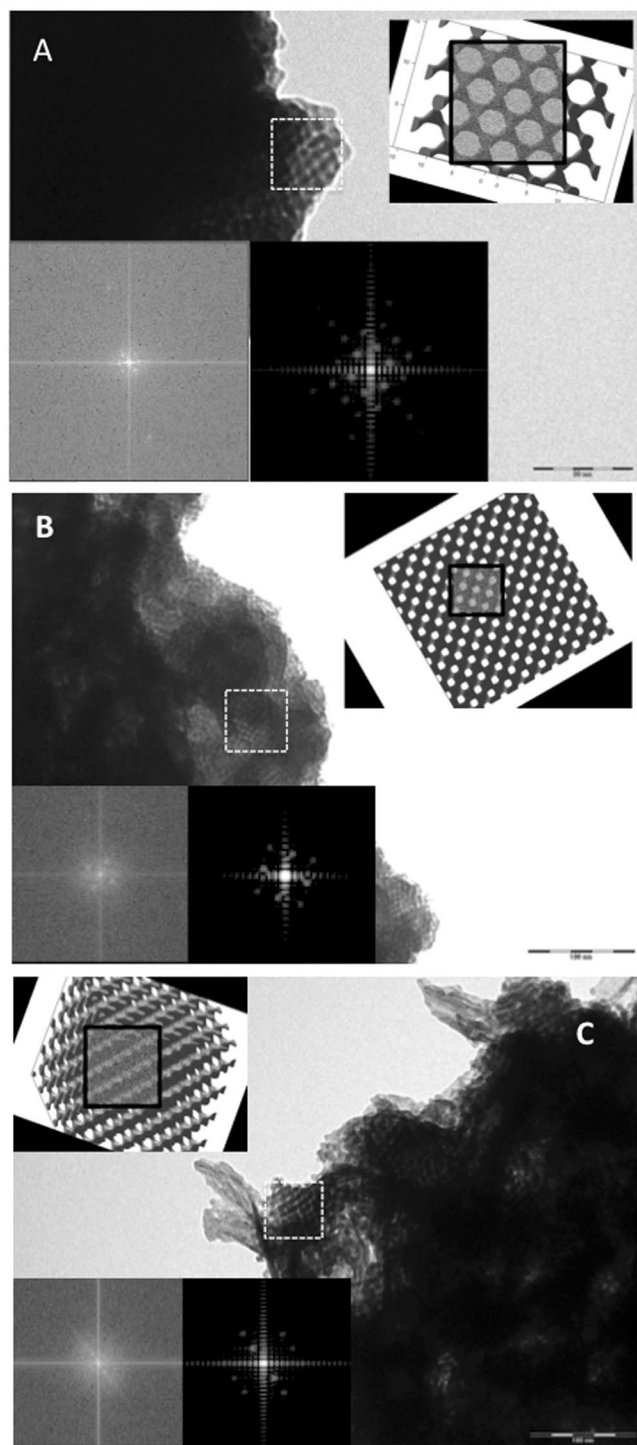


Figure 5. TEM images with corresponding Matlab projections for a single diamond topology nanostructure viewed along the following directions: (A) [110], (B) [100] and (C) non-integer direction perpendicular to [111]. FFTs for each TEM image (bottom left) have been included. For comparison, the corresponding MATLAB projection is shown (top right), with the highlighted rectangular section (with Gaussian noise added artificially) used to produce the corresponding simulated FFT (bottom right).

Phases were indexed by assigning Bragg peaks to known phases. Samples were prepared for transmission electron microscopy by scraping small sections of nanotemplated films with a scalpel over 400 mesh copper transmission electron microscopy grids (Sigma Aldrich). A FEI Tecnai T12 transmission electron microscopy was used to acquire transmission electron microscopy images.

Results and Discussion

The surface morphology of the phytantriol templated bismuth sulphide films was investigated by SEM and a representative image is shown in Fig. 2 which indicates a mostly smooth surface morphology with some pin holes being present. EDX of the phytantriol templated bismuth sulphide films showed a reproducible composition of $40.1 (\pm 5.5)\%$ Bi and $59.9 (\pm 5.5)\%$ S, resulting in a stoichiometry of Bi_2S_3 .

Figure 3 shows a representative grazing incidence X-ray diffraction scan of an electrodeposited Bi_2S_3 film through phytantriol. The diffraction pattern has been indexed in accordance with the pdf card 9007375 for Bismuthinite from the crystallographic open database (COD) which has been superimposed in Fig. 3. There is good agreement between the experimental and theoretical data which indicates that indeed bismuthinite or bismuth sulphide of stoichiometry Bi_2S_3 has formed.

Small angle X-ray scattering (SAXS) in transmission mode and Transmission Electron Microscopy (TEM) were employed to verify and visualize the nanostructures. Figure 4a and b show 1D SAXS radial profiles of the phytantriol modified gold electrode surface prior to electrodeposition (4a), immersed in an electrolyte solution of $100 \text{ mM } \text{Bi}(\text{NO}_3)_3$, $100 \text{ mM } \text{Na}_2\text{S}_2\text{O}_3$ and 200 mM EDTA , and following electrodeposition after removal of phytantriol (4b).

Prior to electrodeposition we can distinguish Bragg peaks with relative positions for $1/d$ in the ratio $\sqrt{2}: \sqrt{3}: \sqrt{4}: \sqrt{6}: \sqrt{8}$ which are representative for the Q224 bicontinuous cubic lattice of phytantriol, with a lattice parameter of $68.9 \pm 0.9 \text{ \AA}$. Following electrodeposition and subsequent removal of phytantriol the 1D SAXS radial profiles reveal a sequence of three distinct and well-resolved Bragg diffraction peaks with $1/d$ spacings in the ratio of $\sqrt{3}: \sqrt{8}: \sqrt{11}$ which are characteristic of a single diamond topology of symmetry $Fd\bar{3}m$ (Q_{227}), with a lattice parameter of $139.6 \pm 3.2 \text{ \AA}$. This corresponds to approximately double the lattice parameter of phytantriol in the electrolyte ($68.9 \pm 0.9 \text{ \AA}$) and is consistent with electrodeposition occurring in one water channel of the double diamond structure, resulting in a single diamond nanostructure³⁰ with a doubled lattice parameter due to a reduction in symmetry as shown in Fig. 1(b).

To provide further evidence TEM images in combination with MATLAB projections are shown in Fig. 5 which reveal a well ordered nanostructure. The MATLAB projections with the highlighted rectangular section (with Gaussian noise added artificially) are then used to produce the corresponding simulated FFT (bottom right) which can be directly compared against the FFTs of the TEM image (bottom left). These are in excellent agreement and also reveal the cubic symmetry of the single diamond structure.

From the MATLAB projections as well as the TEM images the following lattice parameters can be estimated: a) 125 \AA , b) 109 \AA and c) 124 \AA . The lattice parameters based on the simulations therefore matched with a lattice parameter of a similar order of magnitude as those determined by SAXS ($139.6 \pm 3.2 \text{ \AA}$), however, these were smaller by 25%. This may be due to actual shrinkage of the bismuth sulphide films after detachment from the substrates. Nevertheless it can be concluded that within experimental error as evidenced by SAXS and TEM data the formation of a single diamond morphology in nanostructured bismuth sulphide has occurred.

Conclusions

We have demonstrated for the first time that inverse lipid cubic mesophases can act as suitable templates for the room temperature production of highly ordered 3D semiconductor compound nanostructures (bismuth sulphide) as evidenced by SAXS and TEM. Fabrication via this route can be carried out in one step without the need for elaborate and complex synthetic steps resulting in well-ordered materials that are attached to an electrode surface. Hence this therefore represents an important step forward towards the fabrication of nanostructured 3D semiconductors for device applications.

References

1. Xu, S. *et al.* Self-powered nanowire devices. *Nat. Nanotechnol.* **5**, 366–373 (2010).
2. Bonifacio, L. D. *et al.* Towards the photonic nose: a novel platform for molecule and bacteria identification. *Adv. Mater.* **22**, 1351–1354 (2010).
3. Duay, J., Gillette, E., Hu, J. & Lee, S. B. Controlled electrochemical deposition and transformation of hetero-nanoarchitected electrodes for energy storage. *Phys. Chem. Chem. Phys.* **15**, 7976–7993 (2013).
4. Wei, D. *et al.* A nanostructured electrochromic supercapacitor. *Nano Lett.* **12**, 1857–1862 (2012).
5. Crossland, E. J. W., Nedelcu, M., Ducati, C., Ludwigs, S. & Hillmyer, M. A. Steiner, U. and Snaith, H.J., Block copolymer morphologies in dye-sensitized solar cells: probing the photovoltaic structure–function relation. *Nano Lett.* **9**, 2813–2819 (2008).
6. Rauber, M. *et al.* Highly-ordered supportless three-dimensional nanowire networks with tunable complexity and interwire connectivity for device integration. *Nano Lett.* **11**, 2304–2310 (2011).
7. Lee, J. M. *et al.* Vertical Pillar-Superlattice Array and Graphene Hybrid Light Emitting Diodes. *Nano Lett.* **10**, 2783–2788 (2010).
8. Martin, J., Martín-González, M., Fernández, J. H. & Caballero-Calero, O. Ordered three-dimensional interconnected nanoarchitectures in anodic porous alumina. *Nat. Commun.* **5**, 5130–5139 (2014).
9. Eibl, O., Nielsch, K., Peranio, N. & Volklein, F. Eds. In Thermoelectric Bi_2Te_3 nanomaterials, Wiley, Weinheim, (2015).
10. Vukovic, I., Brinke, G. T. & Loos, K. Block copolymer template-directed synthesis of well-ordered metallic nanostructures. *Polymer* **54**, 2591–2605 (2013).
11. Attard, G. S. *et al.* Mesoporous platinum films from lyotropic liquid crystalline phases. *Science* **278**, 838–840 (1997).
12. Crossland, E. J. W. *et al.* A bicontinuous double gyroid hybrid solar cel. *Nano Lett.* **9**, 2807–2812 (2009).
13. Miller, B. & Heller, A. Semiconductor liquid junction solar cells based on anodic sulfide films. *Nature* **262**, 681 (1976).
14. Robin, O., Grimm, J. M., Wojtkiewicz, G. & Weissleder, R. An X-ray computed tomography imaging agent based on long-circulating bismuth sulphide nanoparticles. *Nat. Mater.* **5**, 118–122 (2006).
15. Liufu, S.-C., Chen, L.-D., Yao, Q. & Wang, C.-F. Assembly of one-dimensional Bi_2S_3 nanorods into films with enhanced thermoelectric transport properties. *Appl. Phys. Letts.* **90**, 112106 (2007).
16. Liufu, S.-C., Chen, L.-D., Yao, Q. & Wang, C.-F. Bismuth Sulfide Thin Films with Low Resistivity on Self-Assembled Monolayers. *J. Phys. Chem. B* **110**, 24054–24061 (2006).
17. Medles, M. *et al.* Optical and electrical properties of Bi_2S_3 films deposited by spray pyrolysis. *Thin Solid Films* **497**, 58–64 (2006).
18. Yu, Y., Jin, C. H., Wang, R. H., Chen, Q. & Peng, L.-M. High-Quality Ultralong Bi_2S_3 Nanowires: Structure, Growth, and Properties, *J. Phys. Chem. B*, **109**, 18772–18776, Oct. 2005.

19. Sigman, M. B. & Korgel, B. A. Solventless Synthesis of Bi₂S₃ (Bismuthinite) Nanorods, Nanowires, and Nanofabric. *Chem. Mater.* **7**, 1655–1660 (2005).
20. Lokhande, C. D. & Bhosale, C. H. Electrodeposition of CdS, Bi₂S₃ and Cd-Bi-S thin films and their photoelectrochemical properties. *Bull. Electrochem.* **6**, 662–624 (1990).
21. Yesugade, N. S., Lokhande, C. D. & Bhosale, C. H. Structural and optical properties of electrodeposited Bi₂S₃, Sb₂S₃ and As₂S₃ thin films. *Thin Solid Films* **263**, 145–149 (1995).
22. Georges, C. R. *et al.* Electrochemical Deposition of Bi_[sub 2]S_[sub 3] Thin Films Using Dimethylsulfoxide as a Solvent. *J. Electrochem. Soc.* **154**, D669–D673 (2007).
23. Peng, X. S. *et al.* Electrochemical fabrication of ordered Bi₂S₃ nanowire arrays. *J. Phys. D. Appl. Phys.* **34**, 3224–3228 (2001).
24. Wang, D. *et al.* A general route to macroscopic hierarchical 3D nanowire networks. *Angew. Chem.* **116**, 6295 (2004).
25. Gorishnyy, T. M., Mal'dovan, C., Ullal, C. & Thomas, E. Sound ideas. *Phys. World* **18**, 24–29 (2005).
26. Dolan, J. *et al.* Optical Properties of Gyroid Structured Materials: From Photonic Crystals to Metamaterials. *Adv. Opt. Mat.* **3**, 12–32 (2015).
27. Barauskas, J. & Landh, T. Phase behavior of the phytantriol/water system. *Langmuir* **19**, 9562–9565 (2003).
28. Henrich, B. *et al.* PILATUS: A single photon counting pixel detector for X-ray applications. *Nuclear Instruments and Methods in Physics Research A* **607**, 247–249 (2009).
29. Huang, T. C., Toraya, H., Blanton, T. N. & Wu, Y. X-ray powder diffraction analysis of silver behenate, a possible low-angle diffraction standard. *J. Appl. Cryst.* **26**, 180–184 (1993).
30. Akbar, S., Elliott, J. M., Rittma, M. & Squires, A. M. Facile Production of Ordered 3D Platinum Nanowire Networks with Single Diamond Bicontinuous Cubic Morphology. *Adv. Mater.* **25**, 1160–1164 (2013).

Acknowledgements

We are grateful to Diamond light source for allocation of beam times SM14925 and SI10330 on beam line I22. The authors acknowledge the financial support of equipment grant (EP/K00509X/1) for the SmartLab and financial support for M. Burton (EPSRC industrial CASE award 11330323).

Author Contributions

I.N. wrote the main manuscript text and M.B. provided Figures 1–5. C.L., P.S. and N.T. helped with the acquisition of the SAXS data at beamline I22 at Diamond Light Source, whilst A.S. created the MATLAB simulations and FFTs. N.W. proof-read the manuscript.

Additional Information

Competing Interests: The authors declare that they have no competing interests.

Publisher's note: Springer Nature remains neutral with regard to jurisdictional claims in published maps and institutional affiliations.



Open Access This article is licensed under a Creative Commons Attribution 4.0 International License, which permits use, sharing, adaptation, distribution and reproduction in any medium or format, as long as you give appropriate credit to the original author(s) and the source, provide a link to the Creative Commons license, and indicate if changes were made. The images or other third party material in this article are included in the article's Creative Commons license, unless indicated otherwise in a credit line to the material. If material is not included in the article's Creative Commons license and your intended use is not permitted by statutory regulation or exceeds the permitted use, you will need to obtain permission directly from the copyright holder. To view a copy of this license, visit <http://creativecommons.org/licenses/by/4.0/>.

© The Author(s) 2017